

Journal of Materials Chemistry A

Accepted Manuscript



This is an *Accepted Manuscript*, which has been through the Royal Society of Chemistry peer review process and has been accepted for publication.

Accepted Manuscripts are published online shortly after acceptance, before technical editing, formatting and proof reading. Using this free service, authors can make their results available to the community, in citable form, before we publish the edited article. We will replace this *Accepted Manuscript* with the edited and formatted *Advance Article* as soon as it is available.

You can find more information about *Accepted Manuscripts* in the [Information for Authors](#).

Please note that technical editing may introduce minor changes to the text and/or graphics, which may alter content. The journal's standard [Terms & Conditions](#) and the [Ethical guidelines](#) still apply. In no event shall the Royal Society of Chemistry be held responsible for any errors or omissions in this *Accepted Manuscript* or any consequences arising from the use of any information it contains.



www.rsc.org/materialsA

Effect of Different Lead Precursors in Perovskite Solar Cells Performance and Stability

Fadi Kamal Aldibaja, Laura Badia, Elena Mas-Marzá,^{*} Rafael S. Sánchez, Eva M. Barea and Ivan Mora-Sero^{*}

Photovoltaics and Optoelectronic Devices Group, Departament de Física, Universitat Jaume I, 12071 Castelló, Spain

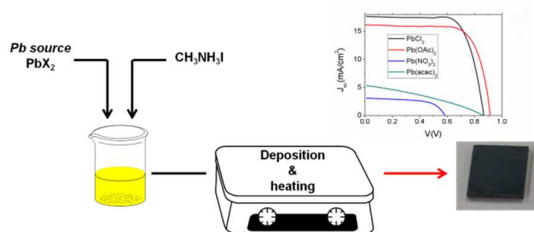
^{*}corresponding authors: E. M.-M.: emas@uji.es, I.M.-S: sero@uji.es

7 December 2014

Abstract

We present the use of halide (PbCl_2) and non-halide lead precursors (Pb(OAc)_2 ($\text{OAc}=\text{CH}_3\text{CH}_2\text{COO}^-$), $\text{Pb(NO}_3)_2$, Pb(acac)_2 ($\text{acac}=(\text{CH}_3\text{COCHCOCH}_3)^-$) and PbCO_3) for the preparation of perovskite solar cells. We have confirmed by X-ray diffraction the growth of $\text{CH}_3\text{NH}_3\text{PbI}_3$ in all the analyzed cases, except for PbCO_3 , independently of the lead precursor used for the synthesis of the perovskite. In addition, different cell configurations, thin film and mesoporous scaffolds, TiO_2 or Al_2O_3 , have also been prepared. We have observed that the lead precursor influences strongly on the structural properties of perovskite (grain size), as well as on the solar cell performance. Photovoltaic conversion efficiencies comparable to those achieved when using the commonly employed PbCl_2 have been obtained with Pb(OAc)_2 as lead source. Stability studies of the perovskite films and devices have also been carried out; demonstrating that the lead precursor also influences this aspect. Stability is strongly affected by atmosphere and illumination conditions, but also by the lead precursor employed for the perovskite synthesis. These results highlight that other lead sources, different to the commonly used PbCl_2 and PbI_2 , are also suitable for the development of PSCs, opening a new way for device performance optimization.

TOC graphic



Key words: Photovoltaics, Solar cells, Perovskite, lead precursors

Introduction

Nowadays, hybrid halide perovskites with general formula ABX_3 , where $X=Cl, Br$ or I , can be considered, without any doubts, an ideal candidate for the preparation of photovoltaic devices. The most successful and commonly used hybrid halide perovskite for photovoltaic applications has been $CH_3NH_3PbI_3$ and its analogue prepared from lead chloride, commonly notated as $CH_3NH_3PbI_{3-x}Cl_x$.¹⁻³ The first example of the use of hybrid halide perovskites in solar cells was reported by Miyasaka in 2009,⁴ and from that moment the field of Perovskite Solar Cells (PSCs) experienced the best ever efficiency enhancement within an outstandingly short period of time.⁵ In 2012, the use of perovskite for photovoltaics took a step forward with the preparation of all-solid devices with spiro-OMeTAD, as selective contact and Hole Transporting Material (HTM), producing 10-11% efficiency.^{6,7} Since then, numerous research groups have focused their efforts on the development of different approaches to optimize this field, mainly based on the use of different cell configurations (TiO_2 or Al_2O_3 scaffolds or planar configurations with no scaffold), use of mixed halide (Br-I) derivatives of $CH_3NH_3PbI_3$,⁸⁻¹⁰ exchange of the organic cation $CH_3NH_3^+$,¹¹⁻¹⁴ use of additives in the HTM^{15, 16} or the use of different selective contacts.¹⁷⁻²⁰ In addition, high efficiency samples have been obtained from a broad variety of deposition techniques, including spin-coating^{6, 7} two step procedures involving dip-coating²¹ or drop casting methods²² and solvent engineering strategies.¹ Besides, evaporation procedures have also been demonstrated to be excellent processes for the preparation of perovskite films.²³

Although perovskites $CH_3NH_3PbI_3$ and $CH_3NH_3PbI_{3-x}Cl_x$ are normally prepared by the reaction in solution of CH_3NH_3I and PbI_2 in 1:1 ratio or CH_3NH_3I and $PbCl_2$ in 3:1 ratio, other non-halide lead precursors as lead acetate, $Pb(OAc)_2$, or lead nitrate, $Pb(NO_3)_2$, are also known to be appropriate candidates for the synthesis of these materials.²⁴⁻²⁶ However, most of these perovskites, synthesized from non-halide precursors, have not been analyzed in complete photovoltaic devices yet. Therefore, in this article we study the performance and stability of PSCs prepared from non-halide lead precursors. These cells were prepared in mesoporous heterojunction configuration glass/FTO/compact TiO_2 /mesoporous scaffold / $CH_3NH_3PbI_3$ /spiro-OMeTAD/Au, with TiO_2 or Al_2O_3 scaffold, and planar configuration glass/FTO/compact TiO_2 / $CH_3NH_3PbI_3$ /spiro-OMeTAD/Au. Performance and stability

have been compared to those obtained with the solar cells prepared with lead chloride precursor, $\text{CH}_3\text{NH}_3\text{PbI}_{3-x}\text{Cl}_x$ as reference. We have observed that the lead precursor employed affects dramatically the perovskite morphology and crystal size, even though the same experimental procedures were followed for the synthesis. Furthermore, preliminary studies of the stability of both perovskite films and PSCs have also been performed and compared with $\text{CH}_3\text{NH}_3\text{PbI}_{3-x}\text{Cl}_x$.

Experimental section

Substrate preparation. Fluorine doped tin oxide (FTO) coated glass substrates (25 x 25 mm, Pilkington TEC15, $\sim 15\Omega/\text{sq}$ resistance) were etched with zinc powder and HCl (2M) to obtain 0.224 cm^2 of active electrode area. The substrates were cleaned with soap (Hellmanex) and rinsed with milliQ water and ethanol. Then, the sheets were sonicated for 15 minutes in a solution of acetone: isopropanol (1:1 v/v), rinsed with ethanol and dried with compressed air. After that, a UV/ozone treatment was performed for 15 minutes. Then, a TiO_2 blocking layer was deposited onto the substrates by spray pyrolysis at 450°C , using a titanium diisopropoxide bis(acetylacetonate) (75% in isopropanol, Sigma-Aldrich) solution diluted in ethanol (1:39, v/v), with oxygen as carrier gas. After the spraying process the films were kept at 450°C for 5 minutes.

Mesoporous TiO_2 layer. When needed, a mesoporous TiO_2 layer was deposited by spin coating at 4000 rpm during 60 s using a TiO_2 paste (Dyesol 18NRT, 20 nm average particle size) diluted in terpineol (1:3, weight ratio). After drying at 80°C , the TiO_2 layers were heated at 470°C for 30 min and cooled to room temperature. The thickness determined by Scanning Electron Microscopy was $\sim 200\text{ nm}$.

Mesoporous Al_2O_3 layer. When needed, the mesoporous Al_2O_3 layer was deposited by spin coating at 2500 rpm. during 60 s using a colloidal dispersion of $< 50\text{ nm}$ Al_2O_3 nanoparticles in isopropanol, followed by drying at 150°C for 30 minutes. The thickness determined by Scanning Electron Microscopy was $\sim 200\text{ nm}$.

Perovskite deposition. The perovskite precursor solution (100 μl), prepared by reacting 2.64 mmol of methylammonium iodide and 0.88 mmol of the corresponding lead precursor at a 3:1 mol ratio in 1 mL of DMF, was spin-coated inside the glove box at 2000 r.p.m. for 60 s. After the deposition, the substrate was kept at 100°C for 10 min. Next, the substrates were heated at 100°C during 1 hour in an oven under air stream.

The lead precursor used in this work are PbCl_2 , $\text{Pb}(\text{OAc})_2$, $\text{Pb}(\text{NO}_3)_2$, $\text{Pb}(\text{acac})_2$ and PbCO_3 .

Hole transport layer (HTM) deposition. A ~300-400 nm-thick of HTM was deposited on top of the perovskite substrates by spin coating at 4000 r.p.m for 30 s under air conditions, using 100 μL of spiro-OMeTAD solution. The spiro-OMeTAD solution was prepared by dissolving 72.3 mg of (2,2',7,7'-tetrakis(N,N'-di-p-methoxyphenylamine)-9,9'-spirobifluorene), 28.8 μL of 4-tert-butylpyridine and 17.5 μL of a stock solution of 520 mg/mL of lithium bis(trifluoromethylsulphonyl)imide in acetonitrile, in 1 mL of chlorobenzene.

Gold electrodes deposition. The deposition of 60 nm of gold was performed by thermal evaporation under ultrahigh vacuum conditions, using a commercial MBraun vacuum chamber. Before beginning the evaporation the chamber was evacuated until pressure of $1 \cdot 10^{-6}$ mbar.

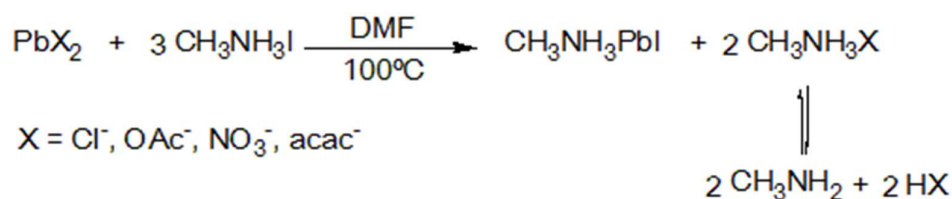
Perovskite films characterization. The morphology and structural properties of the films were analyzed using a JEOL 7001F scanning electron microscope with a film emission gun (SEM-FEG) and a Bruker AXS-D4 Endeavor Advance X-ray diffractometer (XRD) using $\text{Cu K}\alpha$ radiation. The PL spectra of the films were registered by using a spectrophotometer based on a CCD (Andor i-DUS DV420A-OE) coupled with a spectrograph as a diffraction grating (Newport 77400). Commercial laser diode (532 nm, $52 \text{ mW} \cdot \text{cm}^{-2}$) was used as excitation source, whose power intensity was adjusted by means of neutral density filters.

Solar cells characterization. The Incident Photon to Current Efficiency (IPCE) were performed using a Xenon lamp power source coupled with a monochromator controlled by a computer; the photocurrent was measured using an optical power meter 70310 from Oriel Instruments and a Si photodiode to calibrate the system. Current density-voltage (J - V) curves were performed under 1 sun illumination ($100 \text{ mW} \cdot \text{cm}^{-2}$) using a xenon arc lamp simulator (Sun 2000, ABET Technologies) with an AM 1.5 G spectral filter and a Keithley 2400, previously calibrated with an NREL-calibrated Si solar cell. All the measurements were performed with an opaque mask of 0.08 cm^2 and without encapsulation. The electrochemical Impedance spectroscopy measurements were carried out by means of a FRA equipped PGSTAT-30 from Autolab under 1 sun illumination conditions at different applied voltages and applying a 30 mV A/C voltage perturbation

over the constant applied bias with a frequency ranging.

Results and discussion

With the aim to evaluate the possibility of using non-halide lead sources for the synthesis of perovskite films, we have chosen different lead non-halide reagents: $\text{Pb}(\text{OAc})_2$, $\text{Pb}(\text{NO}_3)_2$, $\text{Pb}(\text{acac})_2$ and PbCO_3 . For comparative purposes, we decided to contrast the results obtained with these lead precursor with those achieved in our laboratory with PbCl_2 precursor as reference. Perovskite films were synthesized as explained in the experimental section. These thin films, obtained using the different lead precursors, were analyzed by X-Ray Diffraction (XRD). For this purpose, all the perovskite films were prepared onto mesoporous TiO_2 scaffold, by spin coating of a DMF solution of the corresponding lead precursor and $\text{CH}_3\text{NH}_3\text{I}$ in 1:3 ratio due to stoichiometric reasons. After the deposition, films were annealed at 100°C (exact details in the Experimental section). The fastest formation of perovskite was observed when using $\text{Pb}(\text{OAc})_2$, probably due to the lower melting point of the excess methylammonium acetate, which is formed as a result of the excess of $\text{CH}_3\text{NH}_3\text{I}$ employed, see scheme 1. Reaction of lead source and $\text{CH}_3\text{NH}_3\text{I}$ in a 1:3 ratio, led to the formation of perovskite $\text{CH}_3\text{NH}_3\text{PbI}_3$ and excess of the corresponding methylammonium salt, which was eliminated during the annealing procedure, in the line of the observations realized by other authors.^{27, 28}



Scheme 1: General reactions proposed for the synthesis of $\text{CH}_3\text{NH}_3\text{PbI}_3$ perovskite from different lead precursors.

XRD measurements of the different perovskite films allowed us to confirm that precursors $\text{Pb}(\text{OAc})_2$, $\text{Pb}(\text{NO}_3)_2$ and $\text{Pb}(\text{acac})_2$ are suitable candidates for the preparation of $\text{CH}_3\text{NH}_3\text{PbI}_3$ (see Figure 1). Failure of PbCO_3 in the formation of

perovskite was attributed to its low solubility in DMF, even at 80°C (not shown in Figure 1). In all the cases analyzed in Figure 1, diffraction peaks of $\text{CH}_3\text{NH}_3\text{PbI}_3$ are clearly recognized indicating the formation of this perovskite when using the four different lead precursors. PbCl_2 , $\text{Pb}(\text{OAc})_2$ and $\text{Pb}(\text{NO}_3)_2$ produce $\text{CH}_3\text{NH}_3\text{PbI}_3$ films with preferential (110) orientation, especially the former two, as can be deduced by the relative intensities between diffraction peaks in comparison with a powder samples. As previously observed, the presence of a minor peak at $2\theta \sim 12.75^\circ$ indicates that traces of PbI_2 remain in the film.¹⁷ This peak is sensible reduced when $\text{Pb}(\text{NO}_3)_2$ is used as lead precursor. Presence of PbI_2 phase does not imply necessarily a deleterious effect for device performance, as it has been reported a passivation effect of $\text{CH}_3\text{NH}_3\text{PbI}_3$ by PbI_2 .²⁹ The intensity of this peak increases for $\text{Pb}(\text{acac})_2$, suggesting that in this case the reaction is not completed. Note that different precursors are compared using the same experimental procedures, probably film and subsequent photovoltaic device will require a different optimized preparation procedure for each precursor for an optimum behavior. Moreover, the presence of additional peaks in the XRD spectrum of the perovskite film, corresponding to the substrate (FTO and TiO_2), for $\text{Pb}(\text{acac})_2$ and to a lesser extent in $\text{Pb}(\text{NO}_3)_2$ precursors, suggests that further optimization of the reaction process is needed.

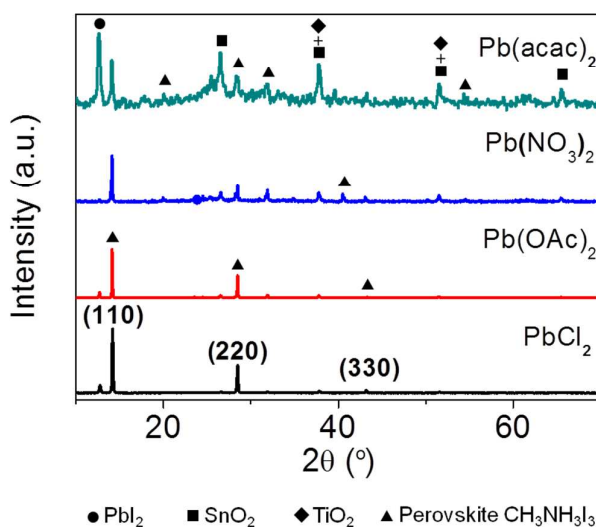


Figure 1: XRD of the films prepared with different lead precursors, with the exception of PbCO_3 that does not produce $\text{CH}_3\text{NH}_3\text{PbI}_3$ with the common synthesis procedure employed.

Absorbance data also proved that perovskite $\text{CH}_3\text{NH}_3\text{PbI}_3$ can be synthesized from the non-halide lead reagents $\text{Pb}(\text{OAc})_2$, $\text{Pb}(\text{NO}_3)_2$ and $\text{Pb}(\text{acac})_2$, by comparison with the spectra obtained when using PbCl_2 . As can be seen in Figure 2a (normalized absorption spectra), all non-halide precursors and reference formed perovskite films that present similar absorption spectra features. However, the absorption signal for $\text{Pb}(\text{NO}_3)_2$ is deformed in comparison with the reference sample. This effect arises from the light scattering of the sample mainly due to the non homogeneous film deposition when using this lead source. Besides, the intensity of the absorption spectrum is significantly lower (Figure S1, Supporting Information), thus suggesting that although perovskite $\text{CH}_3\text{NH}_3\text{PbI}_3$ is formed, further improvement is needed in order to obtain an optimal amount and quality of the perovskite deposited. Additionally, photoluminescence data (Figure 2b) confirmed that all the samples showed the same emission pattern regardless of the lead precursor employed for the perovskite preparation. Curiously, a small shift in the maximum for each emission is observed depending on the lead source, which could be attributed to the different morphology of the perovskite crystal of each film sample. In fact, previous studies revealed a direct influence of the crystal size on the optical properties of the perovskite films.^{30, 31} Particularly, a slight blue-shift of the absorption and photoluminescence signals is observed for small crystallites. In any case, further studies are required for elucidating the fundamentals of this phenomenon; nevertheless these issues are out of the scope of this work.

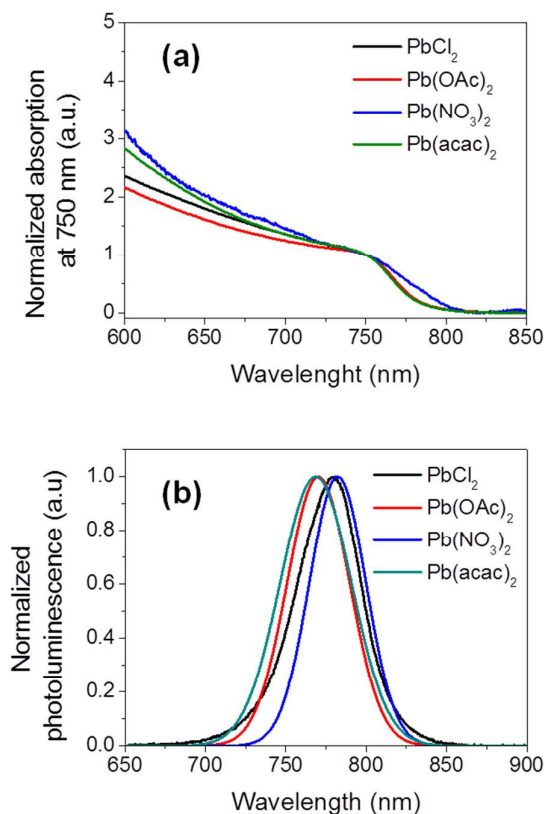


Figure 2: (a) Normalized light absorption at wavelength 750 nm and (b) normalized photoluminescence of the films prepared with different lead precursors.

The morphology of the perovskite films, using Pb(OAc)_2 and PbCl_2 precursors, was analyzed by Scanning Electron Microscope. Figure 3 shows the SEM images taken from samples with and without TiO_2 mesoporous scaffold configuration. Samples prepared with TiO_2 mesoporous scaffold presents an overlayer of perovskite that does not cover completely the mesoporous layer, see Figure 3c and 3d. Interestingly, smaller crystal sizes of perovskite were obtained for the case of Pb(OAc)_2 (in both configurations flat and with mesoporous scaffold), probably due to the fast crystallization, in comparison with PbCl_2 precursor, detected when using this reagent. These results reflect how the type of lead precursor utilized for the growth of $\text{CH}_3\text{NH}_3\text{PbI}_3$ affects dramatically the morphological properties of perovskite layers.

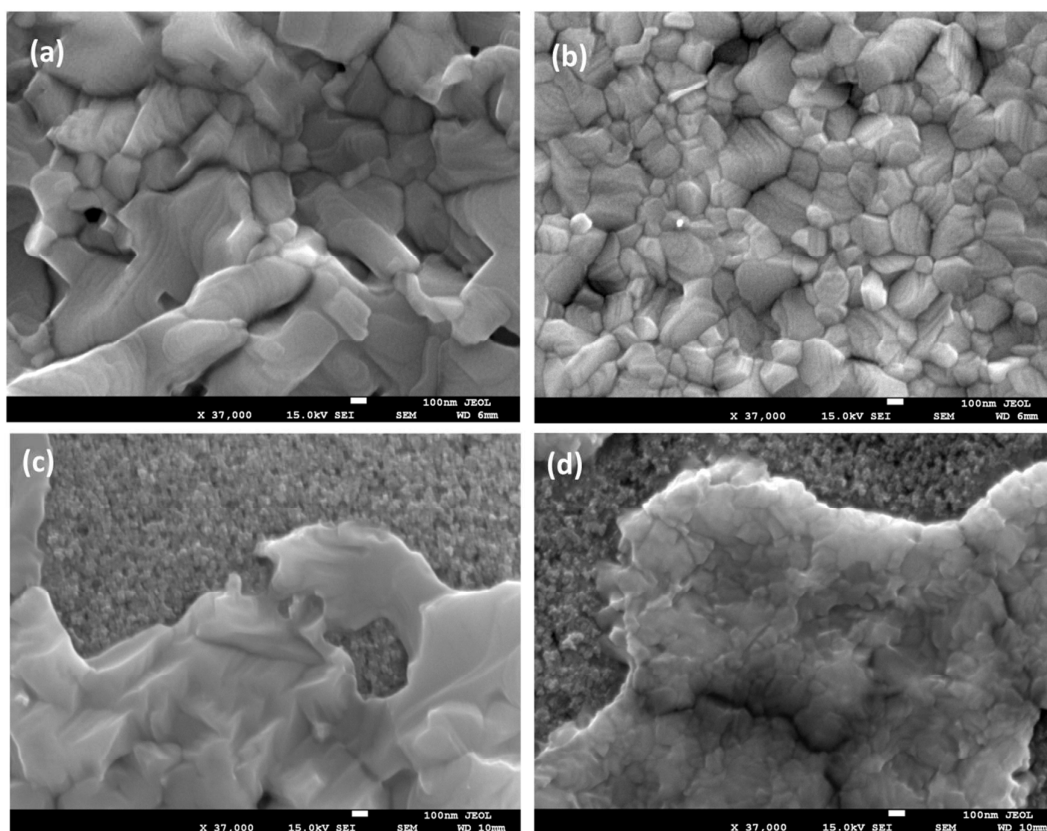


Figure 3: SEM picture of $\text{CH}_3\text{NH}_3\text{PbI}_3$ perovskite layers growth on flat substrate with (a) PbCl_2 and (b) $\text{Pb}(\text{OAc})_2$ lead precursors, and on substrate with mesoporous TiO_2 scaffold with (c) PbCl_2 and (d) $\text{Pb}(\text{OAc})_2$ lead precursors. Scale bar represents 100 nm.

XRD analysis clearly establishes the preparation of perovskite $\text{CH}_3\text{NH}_3\text{PbI}_3$ films from non-halide lead precursors, but different morphological properties have been revealed by SEM micrograph analysis. In order to study the influence on the final photovoltaic performance, PSCs have been prepared using the different lead precursors under study. All devices were prepared using the same experimental procedure (details in Experimental section). Figure 4 and Table 1 present the performance of the best PSCs obtained from each lead precursor. As can be seen, only PSC prepared from $\text{Pb}(\text{OAc})_2$ gave satisfactory results in terms of efficiency, comparable to those obtained with reference PbCl_2 precursor (entry 2 and 1, respectively). On the other hand, $\text{Pb}(\text{NO}_3)_2$ and $\text{Pb}(\text{acac})_2$ gave PSCs with low efficiencies (entries 3 and 4, respectively). These results demonstrate that perovskite for solar cells devices can be prepared from lead sources different to the conventional halide precursor PbCl_2 or PbI_2 . In addition PSC

performance depends dramatically on the lead precursor employed, and optimum performance should require a different optimization of growth conditions and preparation. An important dependence of solar cell efficiency and lead precursor was previously reported for quantum dot sensitized solar cell using PbS as light absorbing material.³² In that case a clear influence of the lead precursor on the trap states was established.

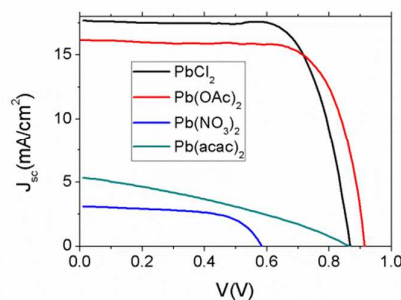


Figure 4: J-V curve for PSCs prepared with different lead precursors using 200 nm of TiO₂ mesoporous scaffold layer. Champion cells obtained for each lead precursor are represented. J-V curves were scanned from positive voltage to zero, at a scan rate of 50 mV·s⁻¹.

Table 1. Solar cell parameters under 1 sun illumination: short circuit current, J_{sc} , open circuit potential, V_{oc} , fill factor, FF, and photoconversion efficiency, η , as obtained from best PSCs performances by using PbCl₂, Pb(OAc)₂, Pb(NO₃)₂ and Pb(acac)₂ as lead sources for the synthesis of the perovskite. Cells were prepared using 200 nm of TiO₂ mesoporous scaffold.

Entry	Precursor	J_{sc} (mA/cm ²)	V_{oc} (V)	FF (%)	Efficiency (%)
1	PbCl ₂	17.67	0.867	72.6	11.1
2	Pb(OAc) ₂	16.2	0.915	72.8	10.8
3	Pb(NO ₃) ₂	3.12	0.584	60.3	1.1
4	Pb(acac) ₂	5.39	0.860	33.3	1.5

Cells using the two precursors presenting the highest efficiencies, PbCl₂ and

Pb(OAc)₂, have been prepared with different configurations, *i.e.* TiO₂ or Al₂O₃ scaffolds or without any scaffold (details in the Experimental section). From the data shown in Table 2, it can be concluded that the best results in terms of efficiency were obtained when using a configuration with a mesoporous TiO₂ layer of 200nm. In all the configurations studied, Pb(OAc)₂ provided lower efficiency than samples prepared with PbCl₂, however it is important to note that the deposition technique employed for both precursors was the same, being this procedures only optimized for PbCl₂. All these results are promising regarding the preparation of high efficiency PSCs from non-halide lead precursor, though additional research is needed to find the optimum deposition conditions, presumably different to the ones employed for PbCl₂. It is noteworthy that the use of Pb(OAc)₂ allowed the preparation of flat perovskite solar cells (without scaffold), whereas this configuration is not straightforward when using PbI₂ instead of PbCl₂.³³ This fact adds an additional degree of versatility in the use of Pb(OAc)₂ as lead source.

Table 2. Different configuration for the PSCs using Pb(OAc)₂ and PbCl₂ as lead sources. IPCE of each cell was measured and integrated, achieving a good agreement with the measured photocurrent obtained in most of the cases.

Entry	Device	J _{sc} (mA/cm ²)	J from IPCE	V _{oc} (V)	FF (%)	Efficiency (%)
1	Flat_PbCl ₂	13.57	13.81	1.023	59.1	8.2
2	Flat_Pb(OAc) ₂	15.11	12.46	0.992	33.5	5.0
3	Al ₂ O ₃ _PbCl ₂	12.35	10.31	1.035	66.9	8.6
4	Al ₂ O ₃ _Pb(OAc) ₂	4.15	2.90	0.940	61.3	2.4
5	TiO ₂ _PbCl ₂	17.67	15.36	0.867	72.6	11.1
6	TiO ₂ _Pb(OAc) ₂	13.48	13.47	0.834	65.5	7.4

Moreover, it is also interesting to highlight that an important cell parameter, open circuit potential, V_{oc} , depends more strongly on PSCs configuration than in the lead precursor employed. Lower V_{oc} is observed when TiO₂ scaffold is used in comparison with samples prepared with Al₂O₃ scaffold or no-scaffold, see Table 2. From Impedance spectroscopy characterization, see Figure 5, it can be clearly observed that at high

applied bias samples with TiO₂ scaffold present lower recombination resistance, R_{rec} , than flat samples, indicating a lower recombination rate for planar cells. Nevertheless, few differences are detected regarding the lead precursors when samples using the same configuration are compared. R_{rec} has been obtained by fitting the impedance spectra with the equivalent circuits previously described.^{10, 34} These results are in good agreement with the lower recombination rate, and consequently higher V_{oc} , observed for CH₃NH₃PbI₃ perovskite in a flat device³⁵ and in samples with Al₂O₃ scaffold,¹⁰ in comparison with samples using TiO₂ scaffold, where just halide lead precursors were used for perovskite formation.

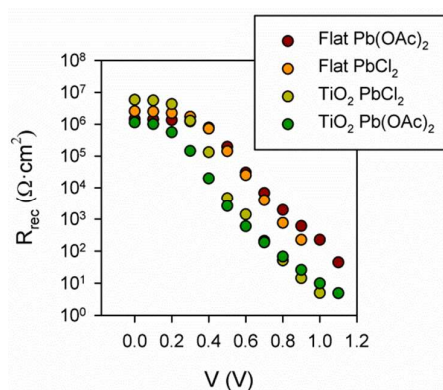


Figure 5: Recombination resistance, R_{rec} , PSCs prepared with Pb(OAc)₂ and PbCl₂ as lead precursors, for flat and TiO₂ scaffold configurations.

The use of different lead precursors brings to the preparation of perovskite layer with different morphological properties, producing photovoltaic devices with different performances. In order to unveil further influence of lead precursors on another important cell issue, such as stability, we have carried out preliminary stability studies of perovskite films and devices under three different conditions of atmosphere and illumination: *i*) air with light (A), *ii*) air without light (B) and *iii*) N₂ atmosphere without light (C). Samples tested in A conditions were leaved under lab ambient illumination. These studies were performed for perovskites obtained from PbCl₂ and Pb(OAc)₂ precursors. Figure 6 shows the cell parameters of the devices prepared and stored under conditions A and B for several days. It can be clearly observed that independently of the precursor, cells stored under ambient lab illumination (conditions A) present a continuous decrease of their efficiency, showing an efficiency just ~20% of the initial one after 15 days of exposure to conditions A. This efficiency decrease can be attributed

mainly to a decrease of photocurrent, and additionally to a reduction of the FF. Noteworthy, the decrease in cell performance is slightly higher in the case of devices prepared from $\text{Pb}(\text{OAc})_2$ than for the analogues from PbCl_2 . Moreover, under dark store conditions instead of lab illumination (conditions B), performance of reference cells, using PbCl_2 precursor, present a good stability after 32 days. However, during this period the efficiency of cells prepared from $\text{Pb}(\text{OAc})_2$ was reduced to $\sim 40\%$ of the initial value. Under conditions C, stability increases even further and efficiencies around 97% and 84% of the initial values are preserved after two months for samples prepared with PbCl_2 and $\text{Pb}(\text{OAc})_2$, respectively (see Supporting Information, Table S1 and Figure S4). This study reflects that lead precursors not only affect the film morphology or cell performance, but also the device stability. These aspects have to be considered for further optimization of cell performance and stability using non-conventional precursors.

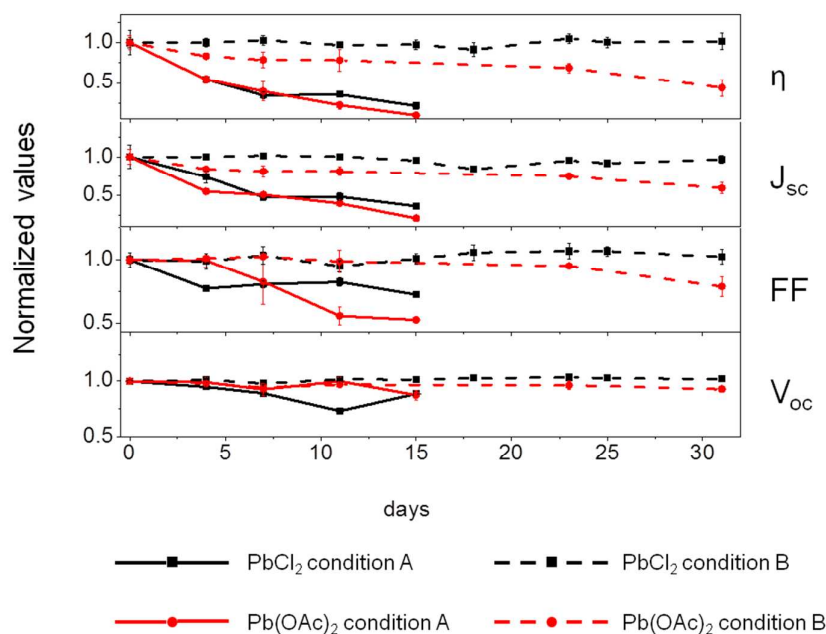


Figure 6: Normalized cell parameters short circuit current, J_{sc} , open circuit potential, V_{oc} , fill factor, FF, and photoconversion efficiency, η , to the values obtained after device preparation (day 0). Parameters measured under 1 sun illumination at different times after preparation. Values represented are average values of 10 samples and error bars indicates the standard deviation. Samples were stored at Conditions A (air with light) and Condition B (air without light). The parameters values were obtained from the J-V curves scanned from positive voltage to zero, at a scan rate of $50 \text{ mV}\cdot\text{s}^{-1}$.

Finally, the stability of the perovskite films, without HTM, was studied by recording the absorption spectra of the perovskite films during 40 days (Figure S5) and taking pictures of them to observe their degradation (Figure S6). Analogous trend to the observed for complete devices has been obtained for perovskite films. These results indicate that the main cause of the lost of efficiency in PSC using spiro-OMeTAD as HTM is the degradation of the perovskite layer. Use of alternative HTL as CuSCN can reduce perovskite degradation.³⁶ It is also important to remark the important effect of photodegradation, in good agreement with previous reports.³⁶ Future development of this technology will require the consideration of these stability issues, where employed precursors play an important role, in addition to the high efficiency.

Literature on the preparation of $\text{CH}_3\text{NH}_3\text{PbI}_3$ PSCs reflects the high versatility of this material, which can be produced from a large variety of preparation methods, being the most relevant: single step solution process,⁷ sequential deposition,²¹ vapor deposition²³ and use of solvent engineering,¹ among others. This versatility has had important consequences as the fast enhancement of the efficiencies reported for PSC has been obtained by an empirical optimization of the perovskite deposition method. In addition to this, in this article we show the existence of another important factor that can affect the perovskite growth process, the precursor employed in the synthesis. In the case of non-halide lead precursors, their corresponding anions are not incorporated into the perovskite structure. However, it does not mean that these anions are mere spectators of the perovskite synthesis, as they affect the final characteristics, from the morphological, optical, electrical and stability point of view.

Another interesting feature affected by the results presented here is related with one of the first discussions that arose in this field, *i.e* the role of Cl in the performance of PSCs. Since the seminal publication of Snaith and Miyasaka⁶ employing PbCl_2 for the preparation of perovskites, there has been an interesting debate about the role of Cl. While some authors have pointed out that Cl is incorporated into the perovskite crystalline structure, which produces $\text{CH}_3\text{NH}_3\text{PbI}_{3-x}\text{Cl}_x$ perovskite instead of the pure iodine $\text{CH}_3\text{NH}_3\text{PbI}_3$, thus slowing down the nucleation dynamics,^{37, 38} others have recently claimed that perovskite prepared from chloride precursor yields to a perovskite films consisting on a combination of $\text{CH}_3\text{NH}_3\text{PbI}_3$ and $\text{CH}_3\text{NH}_3\text{PbCl}_3$.³⁹ However, most

of studies focused on the physical properties of these materials have established that the use of PbCl_2 affects dramatically the properties of perovskite film, such as a significant increase of the diffusion length of free carriers (exceeding $1\mu\text{m}$) and photoluminescence lifetime,^{40, 41} properties that are crucial for the development of high efficient devices. Nevertheless, the exact amount of Cl incorporated in the crystalline structure was very small (below 3–4%)⁴² or even below the detection limit of the techniques employed in the compositional analysis.⁴³ Therefore, the combination of iodide and chloride lead precursors reflects a strong influence of morphology, thus affecting the final cell performance.^{43, 44} Results in this work point in the same direction, extending the influence of the lead precursor on perovskite properties to non-halide precursors.

Conclusions

We have prepared $\text{CH}_3\text{NH}_3\text{PbI}_3$ perovskite films and PSCs using different lead precursors. We have obtained devices with significant efficiency with the non-halide sources $\text{Pb}(\text{NO}_3)_2$, $\text{Pb}(\text{acac})_2$ and $\text{Pb}(\text{OAc})_2$, reaching efficiencies close to the reference cells prepared with PbCl_2 for the case of precursor $\text{Pb}(\text{OAc})_2$. We propose a similar reaction process when a lead precursor different to PbI_2 is used. In that case, a 3:1 molar ratio between $\text{CH}_3\text{NH}_3\text{I}$ and PbX_2 is needed to ensure the final stoichiometry of perovskite $\text{CH}_3\text{NH}_3\text{PbI}_3$. By using this experimental condition, an excess of methylammonium salt remains unreacted, in contrast when using PbI_2 and $\text{CH}_3\text{NH}_3\text{I}$ in 1:1 molar ratio. However, the use of non-iodine lead precursors allows acting in the final properties of the $\text{CH}_3\text{NH}_3\text{PbI}_3$ perovskite films, provoking important implications in the final solar cell performance. We have observed that the morphology of perovskite films, the photoconversion efficiencies and the stability of the devices are strongly influenced by the lead precursor used. The use of $\text{Pb}(\text{OAc})_2$ precursor has produced cells with efficiencies very close to the reference samples prepared with PbCl_2 , being a promising precursors for further improvement of PSCs performance, but presenting lower long term stability than reference. The preparation of PSCs from non-halide lead precursors, different to the normally used PbI_2 and PbCl_2 , clarifies some former questions on perovskite synthesis and properties. The use of non-halide sources opens a new research line in concordance with the use of non-passive reactants for the optimization of this kind of solar cells. These non-passive reactants might affect the final film properties, not only in terms of efficiency but also in stability.

Acknowledgement

The work was supported by MINECO of Spain under project MAT2013-47192-C3-1-R), Universitat Jaume I project 12I361.01/1, E.M.-M thanks the Ramón y Cajal program, R.S.S. thanks the FP7 European project ALLOXIDE (309018).

References

1. N. J. Jeon, J. H. Noh, Y. C. Kim, W. S. Yang, S. Ryu and S. I. Seok, *Nat Mater*, 2014, **13**, 897-903.
2. N.-G. Park, *The Journal of Physical Chemistry Letters*, 2013, **4**, 2423-2429.
3. H. J. Snaith, *The Journal of Physical Chemistry Letters*, 2013, **4**, 3623-3630.
4. A. Kojima, K. Teshima, Y. Shirai and T. Miyasaka, *Journal of the American Chemical Society*, 2009, **131**, 6050-+.
5. http://www.nrel.gov/ncpv/images/efficiency_chart.jpg
6. M. M. Lee, J. Teuscher, T. Miyasaka, T. N. Murakami and H. J. Snaith, *Science*, 2012, **338**, 643-647.
7. H.-S. Kim, C.-R. Lee, J.-H. Im, K.-B. Lee, T. Moehl, A. Marchioro, S.-J. Moon, R. Humphry-Baker, J.-H. Yum, J. E. Moser, M. Gratzel and N.-G. Park, *Sci. Rep.*, 2012, **2**.
8. E. Edri, S. Kirmayer, D. Cahen and G. Hodes, *The Journal of Physical Chemistry Letters*, 2013, **4**, 897-902.
9. J. H. Noh, S. H. Im, J. H. Heo, T. N. Mandal and S. I. Seok, *Nano Letters*, 2013, **13**, 1764-1769.
10. B. Suarez, V. Gonzalez-Pedro, T. S. Ripolles, R. S. Sanchez, L. Otero and I. Mora-Sero, *Journal of Physical Chemistry Letters*, 2014, **5**, 1628-1635.
11. G. E. Eperon, S. D. Stranks, C. Menelaou, M. B. Johnston, L. M. Herz and H. J. Snaith, *Energy & Environmental Science*, 2014, **7**, 982-988.
12. F. C. Hanusch, E. Wiesenmayer, E. Mankel, A. Biniek, P. Angloher, C. Fraunhofer, N. Giesbrecht, J. M. Feckl, W. Jaegermann, D. Johrendt, T. Bein and P. Docampo, *The Journal of Physical Chemistry Letters*, 2014, **5**, 2791-2795.
13. T. M. Koh, K. Fu, Y. Fang, S. Chen, T. C. Sum, N. Mathews, S. G. Mhaisalkar, P. P. Boix and T. Baikie, *The Journal of Physical Chemistry C*, 2013, **118**, 16458-16462.
14. N. Pellet, P. Gao, G. Gregori, T.-Y. Yang, M. K. Nazeeruddin, J. Maier and M. Grätzel, *Angewandte Chemie International Edition*, 2014, **53**, 3151-3157.
15. L. Badia, E. Mas-Marzá, R. S. Sánchez, E. M. Barea, J. Bisquert and I. Mora-Seró, *APL Materials*, 2014, **2**, -.
16. J. H. Noh, N. J. Jeon, Y. C. Choi, M. K. Nazeeruddin, M. Gratzel and S. I. Seok, *Journal of Materials Chemistry A*, 2013, **1**, 11842-11847.
17. S. Chavhan, O. Miguel, H.-J. Grande, V. Gonzalez-Pedro, R. S. Sanchez, E. M. Barea, I. Mora-Sero and R. Tena-Zaera, *Journal of Materials Chemistry A*, 2014, **2**, 12754-12760.
18. J. A. Christians, R. C. M. Fung and P. V. Kamat, *Journal of the American Chemical Society*, 2013, **136**, 758-764.
19. P. Qin, S. Tanaka, S. Ito, N. Tetreault, K. Manabe, H. Nishino, M. K. Nazeeruddin and M. Grätzel, *Nat Commun*, 2014, **5**.
20. H. Zhou, Q. Chen, G. Li, S. Luo, T.-b. Song, H.-S. Duan, Z. Hong, J. You, Y. Liu and Y. Yang, *Science*, 2014, **345**, 542-546.
21. J. Burschka, N. Pellet, S.-J. Moon, R. Humphry-Baker, P. Gao, M. K.

- Nazeeruddin and M. Graetzel, *Nature*, 2013, **499**, 316-+.
22. J.-H. Im, I.-H. Jang, N. Pellet, M. Grätzel and N.-G. Park, *Nat Nano*, 2014, **9**, 927-932.
 23. M. Liu, M. B. Johnston and H. J. Snaith, *Nature*, 2013, **501**, 395-+.
 24. A. Buin, P. Pietsch, J. Xu, O. Voznyy, A. H. Ip, R. Comin and E. H. Sargent, *Nano Letters*, 2014.
 25. D. T. Moore, H. Sai, K. Wee Tan, L. A. Estroff and U. Wiesner, *APL Materials*, 2014, **2**, 081802.
 26. A. Poglitsch and D. Weber, *Journal of Chemical Physics*, 1987, **87**, 6373-6378.
 27. A. Dualeh, P. Gao, S. I. Seok, M. K. Nazeeruddin and M. Grätzel, *Chemistry of Materials*, 2014, **26**, 6160-6164.
 28. Y. Zhao and K. Zhu, *Journal of the American Chemical Society*, 2014, **136**, 12241-12244.
 29. Q. Chen, H. Zhou, T.-B. Song, S. Luo, Z. Hong, H.-S. Duan, L. Dou, Y. Liu and Y. Yang, *Nano Lett.*, 2014, **14**, 4158-4163.
 30. V. D’Innocenzo, G. Grancini, M. J. P. Alcocer, A. R. S. Kandada, S. D. Stranks, M. M. Lee, G. Lanzani, H. J. Snaith and A. Petrozza, *Nat Commun*, 2014, **5**.
 31. M. De Bastiani, V. D’Innocenzo, S. D. Stranks, H. J. Snaith and A. Petrozza, *APL Materials*, 2014, **2**, -.
 32. V. Gonzalez-Pedro, C. Sima, G. Marzari, P. P. Boix, S. Gimenez, Q. Shen, T. Dittrich and I. Mora-Sero, *Physical Chemistry Chemical Physics*, 2013, **15**, 13835-13843.
 33. H.-S. Kim, I. Mora-Sero, V. Gonzalez-Pedro, F. Fabregat-Santiago, E. J. Juarez-Perez, N.-G. Park and J. Bisquert, *Nat Commun*, 2013, **4**.
 34. E. J. Juarez-Perez, R. S. Sanchez, L. Badia, G. Garcia-Belmonte, Y. S. Kang, I. Mora-Sero and J. Bisquert, *The Journal of Physical Chemistry Letters*, 2014, **5**, 2390-2394.
 35. V. Gonzalez-Pedro, E. J. Juarez-Perez, W.-S. Arsyad, E. M. Barea, F. Fabregat-Santiago, I. Mora-Sero and J. Bisquert, *Nano Letters*, 2014, **14**, 888-893.
 36. S. Ito, S. Tanaka, H. Vahlman, H. Nishino, K. Manabe and P. Lund, *ChemPhysChem*, 2014, **15**, 1194-1200.
 37. H. Yu, F. Wang, F. Xie, W. Li, J. Chen and N. Zhao, *Advanced Functional Materials*, 2014, **24**, 7102-7108.
 38. S. T. Williams, F. Zuo, C.-C. Chueh, C.-Y. Liao, P.-W. Liang and A. K. Y. Jen, *ACS Nano*, 2014, **8**, 10640-10654.
 39. B.-w. Park, B. Philippe, T. Gustafsson, K. Sveinbjörnsson, A. Hagfeldt, E. M. J. Johansson and G. Boschloo, *Chemistry of Materials*, 2014, **26**, 4466-4471.
 40. S. D. Stranks, G. E. Eperon, G. Grancini, C. Menelaou, M. J. P. Alcocer, T. Leijtens, L. M. Herz, A. Petrozza and H. J. Snaith, *Science*, 2013, **342**, 341-344.
 41. E. Edri, S. Kirmayer, A. Henning, S. Mukhopadhyay, K. Gartsman, Y. Rosenwaks, G. Hodes and D. Cahen, *Nano Lett.*, 2014, **14**, 1000-1004.
 42. S. Colella, E. Mosconi, P. Fedeli, A. Listorti, F. Gazza, F. Orlandi, P. Ferro, T. Besagni, A. Rizzo, G. Calestani, G. Gigli, F. De Angelis and R. Mosca, *Chemistry of Materials*, 2013, **25**, 4613-4618.
 43. S. Dharani, H. A. Dewi, R. R. Prabhakar, T. Baikie, C. Shi, D. Yonghua, N. Mathews, P. P. Boix and S. G. Mhaisalkar, *Nanoscale*, 2014, **6**, 13854-13860.
 44. Y. Zhao and K. Zhu, *The Journal of Physical Chemistry C*, 2014, **118**, 9412-9418.